Cascaded Fiber-Optic Interferometers for Multi-Perimeter-Zone Intrusion Detection With a Single Fiber Used for Each Defended Zone

Yuan-Hung Lin, Bo-Hong Zheng, and Likarn Wang

***Abstract*—A new fiber-optic perimeter intrusion detection system employing only one single-mode fiber as a disturbance sensor for each perimeter zone is presented. A disturbance signal generated through interference between lights from two resonators, i.e., a linear laser cavity and an extended resonator, was used for determining intrusion for each defended zone. A single-mode fiber was used not only for sensing the intrusion-induced disturbance but also for transmission of pump and signal lights. Although many papers have reported multi-perimeter-zone intrusion detection systems, the study presents, for the first time, a system with a single-mode fiber used all along the perimeter that is in a line pattern and is sectioned into multiple defended zones. An outdoor test for a four perimeter-zone intrusion detection system was carried out with a short section of fiber attached on a netted fence in each defended zone. Experimental results demonstrated that there was no cross interference between any two defended-zone light circuits, and that a high alarm-upon-intrusion rate and a zero false alarm rate could be reached by using the presented detection algorithm.**

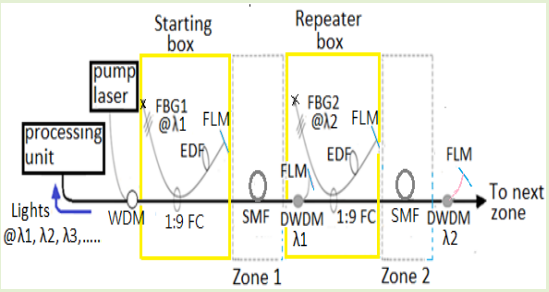

***Index Terms*—Perimeter intrusion detection, multiple defended zones, linear laser cavity, extended resonator, pump laser, erbium-doped fiber.**

I. Introduction

FIBER-OPTIC perimeter intrusion detection systems have attracted much attention of researchers from both academia and industry. Fiber cables can be deployed on fences or walls, or buried underground to sense the intruder-induced disturbance on fibers. Many algorithms have been developed for detecting and locating the intruders against nuisance induced by various sources, such as mechanic acoustic waves, small animals, rain droplets, hailstones, strong winds, etc., which would all cause a strain on the sensing fiber.

A commonly-used intrusion detection system may be configured to have fiber Bragg gratings for detecting the intrusion-induced strain [1], [2], or comprise an optical interferometer such as a Michelson interferometer [3]–[5], a dual Mach-Zehnder interferometer type [6]–[8], and a Sagnac interferometer [9], [10] to sense the disturbance on fibers. Besides, a system with merged Sagnac and Michelson interferometers [11], and a system with combined Sagnac and Mach-Zehnder interferometers [12], [13] have also been research topics for detecting and locating the disturbance applied on a fiber. These two types of systems use two signals to derive the position of the disturbance with a high spatial resolution. However, it should be noted that use of the Sagnac interferometer could have a problem of insensitive detection zone, which occurs near the middle of the Sagnac loop. Although dual Mach-Zehnder types of interferometers have been studied for years, they can only detect a single intrusion event at one time, although some researchers claimed multiple events could be simultaneously detected [14], [15].

Phase-sensitive optical time domain reflectometers (φ-OTDRs) have also been widely used to determine the location of the disturbance on a fiber [16]–[20]. Although such OTDR-based systems can detect multiple events occurring simultaneously along a long-range perimeter with a high spatial resolution, they usually involve the use of relatively sophisticated circuits in event determination. On the other hand, there are many researches focusing on intrusion detection for multiple perimeter zones with each perimeter zone operating independently [21]–[25]. In such detection systems, an alarm can be triggered once any of the perimeter

Manuscript received December 8, 2020; revised January 23, 2021; accepted February 11, 2021. Date of publication February 16, 2021; date of current version April 5, 2021. This work was supported by the Ministry of Science and Technology, Taiwan, under Grant 108-2221-E-007-093. The associate editor coordinating the review of this article and approving it for publication was Dr. Anuj K. Sharma. *(Corresponding author: Likarn Wang.)*

The authors are with the Institute of Photonics Technologies, National Tsing Hua University, Hsinchu 300, Taiwan (e-mail: mark70715@gmail.com; ddgg002008@gmail.com; lkwang@ee.nthu.edu.tw).

Digital Object Identifier 10.1109/JSEN.2021.3059645

zones is invaded with a spatial resolution defined by the length of each perimeter zone. Some detection algorithms for reducing nuisance alarm rates and achieving high intrusion-determining rates can be found [26], [27]. To reduce the cost of multi-zone detection systems, least number of fiber cores (i.e., the single-mode fiber) contained in the fiber cable as well as key optical components were required. The system proposed by [24] used two fibers for disturbance sensing for each perimeter zone; however, the fibers were erbium-doped fibers, which are more expensive than regular fibers. The work in [21] reported a method of using a multiplexed light source distributed among a plurality of defended zones, however with a problem of optical power insufficiency for a large number of defended zones. Inventors of [22] presented a similar method in which multiple laser sources with different wavelengths were used to supply a light for each defended zone at an individual wavelength. The works in [28] and [29] demonstrated different types of multiple-zone intrusion detection for linearly-arranged perimeter zones with, respectively, only three and two fibers employed for each defended zone. The optical circuit for each defended zone in these two works contained a fiber laser cavity with a Michelson interferometer used as a modulator to detect the disturbance on the fibers.

Most of the aforementioned multi-perimeter-zone intrusion detection systems, except those reported in [24] and [29], used three or even more fibers for disturbance sensing as well as light transporting. In this paper, a method of using only one fiber for simultaneous disturbance sensing and light transporting is presented for the first time. In this new method, each defended zone contains a disturbance sensor that is composed of an optical interferometer formed by the circuits of two laser resonators. The new system is outlined in section two, where the principle of operation of the system is also described. Section three presents experimental results for a case of four perimeter zones. A conclusion is then given in section four.

II. Outline of the Presented System

A system of four perimeter zones (or defended zones) is outlined, and the operational principle of the system is also described here.

A. Description of Optical System

Before describing the operation of multi-perimeter-zone system, we explain how each perimeter-zone system works. Each perimeter-zone contains only one single-mode fiber (SMF) for disturbance sensing or intrusion detection. Figure 1 shows the basic optical circuit of each perimeter-zone system, which contains two laser resonators; the first one (denoted as laser cavity hereafter) comprises a cavity with a section of erbium-doped fiber (EDF) situated between a fiber Bragg grating (FBG with the Bragg wavelength λi) and a fiber loop mirror (FLM); and the second resonator (denoted as extended resonator hereafter) is formed by the cavity extended by a combination of a thin film based bandpass filter (DWDM at λi) and an FLM. The EDF is pumped by a 1470 nm pump light

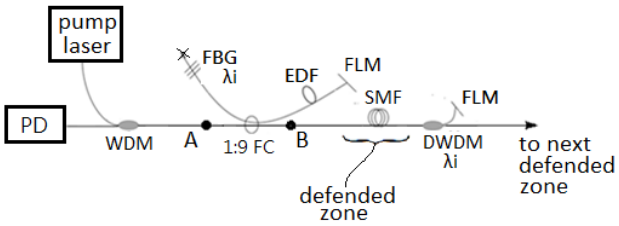

Fig. 1. One defended zone system with one single-mode fiber used for intrusion detection. PD: photodetector, WDM: 1470/1550 WDM coupler, FBG: fiber Bragg grating with a Bragg wavelength of λi, 1:9 FC: 10/90 fiber coupler, EDF: erbium-doped fiber, FLM: fiber loop mirror, SMF: single-mode fiber, DWDM: thin film based bandpass filter at λi. Note that points A and B denote the positions for explanation of system operation given in the text. The symbol x denotes a bending for avoiding end reflection.

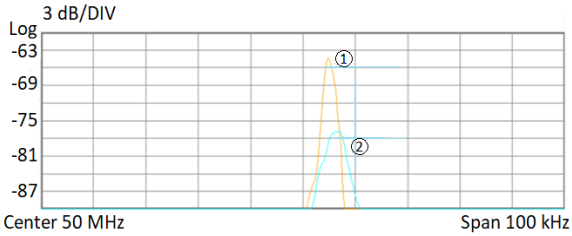

Fig. 2. Measured instantaneous (①) and average (②) spectra of the laser light at the input end of the photodetector, using a self-delayed heterodyne method.

supplied through a 1470/1550 WDM coupler (WDM). The pump light then passes through a 10/90 fiber coupler (1:9 FC) with 10% input pump power directed to the EDF, while the other 90% propagates through the SMF (which is the sensor) and the DWDM, and then partially goes to the laser cavity of the next defended zone. All the optical components beside the SMF of the defended zone are enclosed in protective boxes, which are named "starting box", "repeater box" or "ending box" depending on their positions as shown in Fig. 3.

The light oscillates in the laser cavity at the wavelength defined by the Bragg wavelength λi of the FBG. This laser cavity gives an output light at position A. The output light then transmits through the WDM coupler, and is received by a photodetector (PD). Another part of the laser light is outputted at the other end of the 1:9 FC (i.e., position B), and then propagates down the SMF, passes through the DWDM, and is directed to the FLM at the passband wavelength λi. The light is soon reflected by this FLM and then passes through the DWDM/SMF again, and subsequently reaches the 1:9 FC and enters the laser cavity. This light oscillates between the two end reflectors (i.e., FBG and FLM) of the laser cavity, and then repeatedly emits a part of light at position B, cycling light propagation between the laser cavity and the DWDM/FLM then. The path between point B and DWDM/FLM constitutes an optical path for an extended resonator. This extended resonator would generate an output light at position A, which interferes with the light emitted from the laser cavity that was mentioned in the beginning. The two interfering lights differ from each other mainly in optical path length. The path length difference between the two lights corresponds to the length of the SMF, i.e., the length of the defended zone. The length could be several tens of meters up to several hundreds of

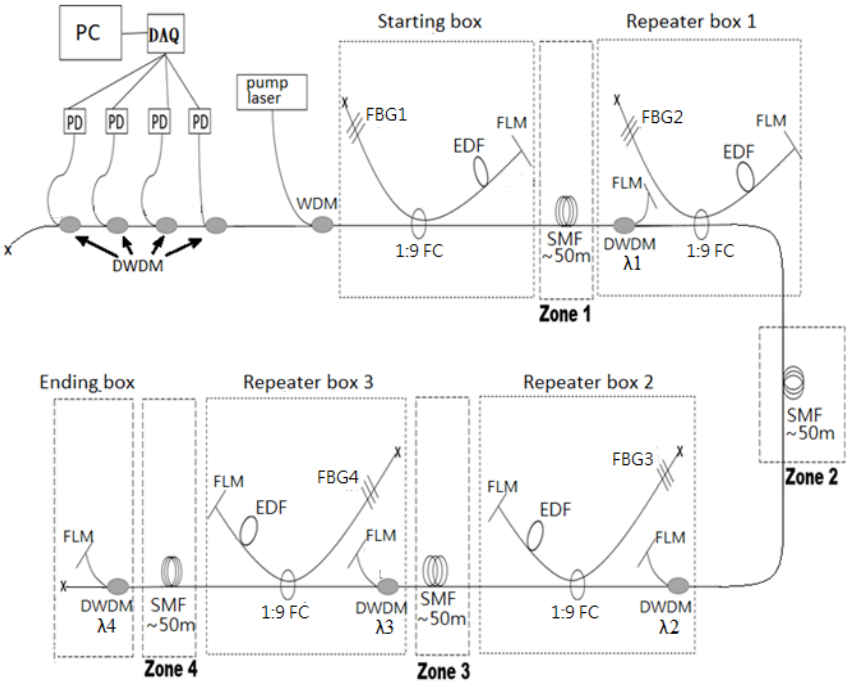

Fig. 3. The presented intrusion detection system that contains 4 perimeter zones separated by repeater boxes. PC: personal computer, DAQ: data acquisition card, PD: photodetector, DWDM: thin film based bandpass filter, WDM: 1480/1550 WDM coupler, FBG:fiber Bragg grating, EDF: erbium-doped fiber, FLM: fiber loop mirror, SMF: single-mode fiber. Here, these DWDMs have passband wavelengths of $\lambda 1 = 1551.72$ nm (at the Bragg wavelength of FBG1), $\lambda 2 = 1554.94$ nm(at the Bragg wavelength of FBG2), $\lambda 3 = 1553.33$ nm(at the Bragg wavelength of FBG3), $\lambda 4 = 1550.12$ nm(at the Bragg wavelength of FBG4). Note that the figure is drawn not to scale.

meters, depending on a practical need. We have measured the laser linewidth of the light at the input end of the PD for the case of 50-meter SMF, using a self-delayed heterodyne method with an offset length of 50 km between the two arms of a Mach-Zehnder interferometer used. The ESA spectrum is shown in Fig.2, where both instantaneous and average spectra are shown, revealing an average linewidth of 2 kHz, which corresponds to a coherence length of ~32 km for the laser light ascertaining that the two aforementioned lights can interfere well. Therefore, any disturbance on the SMF would cause a strain and henceforth a variation in the offset phase between the two lights. And in this case, a variation of optical power can be detected by the PD. A four-perimeter-zone intrusion detection system is shown in Fig.3, where defended-zones are denoted as zones 1 to 4. Note that the figure is drawn not to scale. Different wavelengths are allocated for use in these four zones, i.e., λi is for zone i (i = 1, 2, 3, and 4). A pump laser transmits its optical power down the four sections of SMF and 10 % of the incident power of the 1:9 FC is tapped into each laser cavity and pump the EDF therein. A starting box, an ending box and three repeater boxes are used to enclose all the optical components necessary for implementing laser cavities as well as extended resonators. It is worth noting that DWDM/FLM at λi (here i =1, 2, and 3) used for zone i stays in the same box as the laser cavity used for zone i+1. For instance, the laser cavity used for zone 2 is enclosed in repeater box 1 with DWDM/FLM used for zone 1.

As mentioned previously, when each SMF is disturbed, a light power returning from each defended zone would vary and such a variation of power is then detected as disturbance signal. Different lights from different defended zones are dropped by different DWDM (dense wavelength division multiplexing) thin-film based filters. Here these filters work as drop filters, directing each disturbance signal light to a photodetector (PD). The four detected signals are then inputted to a data acquisition card (DAQ) and then transmit to a personal computer (PC) for signal analysis. Note that the optical power received by the PD should be large enough to give a good signal-to-noise ratio.

B. Algorithm for Intrusion Determination

All disturbance signals delivered back to the PC will be analyzed in real time to see if the signals correspond to an intrusion. All four disturbance signals will be simultaneously checked by the PC in every time period of 1.024 second. Three parameters are calculated from each time-domain disturbance signal: interference visibility (denoted as Visibility), frequency ratio (FR) and level crossing count (LCC).

Visibility is commonly used in the field of optics, which is taken here to identify the strength of the disturbance on a fiber.

It is defined by

$$\text{Visibility} = \frac{V_{\max} - V_{\min}}{V_{\max} + V_{\min}} \tag{1}$$

Disturbances caused by man-made intrusion would induce a larger Visibility than that induced by nuisance sources like temperature variation, wind, sound, small animals and so on. Therefore, a threshold value for Visibility can be set to discriminate a non intrusion case from a man-made intrusion

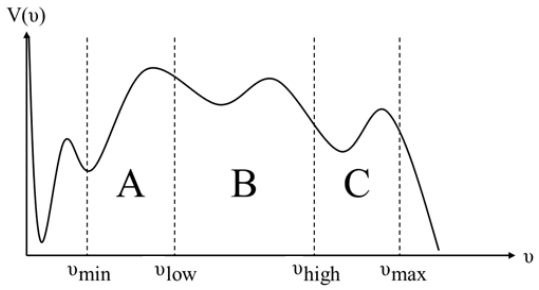

Fig. 4. Fourier spectrum of a disturbance signal with three areas under the spectral curve for three intervals, respectively.

case [28], [29]. Even nuisance sources could induce a large Visibility sometimes, the other two parameters, i.e., FR and LCC, may not be as large as in the case of intrusion.

Frequency ratio (FR) is defined by

$$\mathrm{FR} = \frac{\int_{\upsilon \mathrm{low}}^{\upsilon \mathrm{high}} \mathrm{V}(\upsilon) d\upsilon}{\int_{\upsilon \mathrm{min}}^{\upsilon \mathrm{max}} \mathrm{V}(\upsilon) d\upsilon} \tag{2}$$

where $\mathrm{V}(\upsilon)$ is the spectrum obtained via fast Fourier transform of the time-domain disturbance signal, υ_{min}, υ_{max}, υ_{low} and υ_{high} are the limits of integration defined in Fig.4, where A, B, and C represent, respectively, the areas under the spectral curve over specified intervals. FR is then equal to B/(A+B+C). Usually, a man-made intrusion by maliciously touching, climbing or cutting a netted fence produces a more portion of high frequency components than nuisance sources do. Thus, choosing an area B that covers a little higher frequency interval can rule out the effect of nuisance sources. And therefore a man-made intrusion gives a larger FR than nuisance sources. In this study we chose $\upsilon_{\mathrm{min}} = 1$ Hz, $\upsilon_{\mathrm{max}} = 5000$ Hz, $\upsilon_{\mathrm{low}} = 3000$ Hz, and $\upsilon_{\mathrm{high}} = 5000$ Hz.

LCC is defined as the number of times for the signal voltage to cross upwards a predefined voltage level, which is usually equivalent to the frequency of a sinusoidal signal. For a sudden vibration of the fiber cable that lasts for only a short time period (e.g., less than 1.024 second), some high frequency components may appear in the Fourier spectrum of the disturbance signal. However, LCC may not be large enough because the level crossing count may be small most of the time and that brings down the overall LCC. This case may occur when hailstones periodically strike the fiber cable or when a big bird suddenly takes off from the fiber cable. These cases and the like should be excluded and not be considered as intrusions. Therefore, by setting a proper threshold value for the LCC, one can rule out these possibilities because the detected LCC will not exceed the threshold.

In the study, we made each defended zone have only a small length of fiber cable attached on a netted fence and the other majority part of fiber cable just laid on the grass. We first determined the threshold values for the three parameters for each defended zone. For each defended zone, the three parameters calculated through computer software must all exceed their respective thresholds to claim an intrusion on a real-time basis. After finding the three thresholds for each defended zone, we then tested all the defending systems by determining the false alarm rate and the alarm-upon-intrusion rate for each defended zone. All tests were carried out outdoors.

III. Experiments and Results

A. Description of Fiber System

A four-defended-zone intrusion detection system with the optical circuit shown in Fig.3 was tested. The Bragg wavelengths of the FBGs for the four laser cavities were $\lambda 1 =$ 1551.72 nm (FBG1), $\lambda 2 =$ 1554.94 nm (FBG2), $\lambda 3 =$ 1553.33 nm (FBG3), and $\lambda 4 =$ 1550.12nm (FBG4), respectively. The DWDM thin film based filters used for extended resonators in the defended zones and drop filters at the detector site each had a corresponding wavelength of λi (i = 1,2,3, or 4), and all had a 3-dB bandwidth of ~1.3 nm. The reflection bandwidths and optical reflectivities of all the FBGs were 0.25 nm and 90%, respectively. The wide-bandwidth characteristics of the DWDM thin film based filters ensured that the DWDM filters matched the corresponding FBGs in wavelength against a substantial temperature-induced variation in the Bragg wavelength of each FBG. The pump laser provided an optical power of 160 mW at ~1470 nm, and supplied powers of 14.2 mW, 11.1 mW, 9.3 mW and 7.6 mW to the EDFs in the laser cavities of zone 1, zone 2, zone 3, and zone 4, respectively. It should be noted that the optical power delivered to each EDF was a little lower than expected mainly due to optical losses incurred at the DWDM thin film based bandpass filters. The EDF used here had an absorption coefficient of 5.0~5.6 (6.0~8.0) dB/m at 980 (1530) nm, and the length of the EDF in each laser cavity was 10 m.

The fiber cable deployment for the four-defended-zone intrusion detection system is shown in Fig.5, where four netted fences (name as fences 1 to 4) and all the boxes that housed the required optical components are marked. Fiber cables for the four defended zones are also marked separately by different symbols on the lines. It should be noted that only one single-mode fiber in the fiber cable was used for intrusion detection in each perimeter zone. The length of the fiber cable for each defended zone was about 50 m. It can be seen that only a small part of the fiber cable was attached on the netted fence for each defended zone. Figure 6 shows the four netted fences built outdoors for the experiment. Fences 1,2 and 4 were of soft type nets all with the dimensions of 90 cm(W) × 50 cm(H) as shown in Fig.6(a); while fence 3 (Fig.6(b)) was of 120 cm(W) × 70 cm(H) with a little harder net. Note that the fiber cable hung in the air on both sides of each fence so that it could swing with the wind, and that most parts of the fiber cable lying on the grass were actually suspended and were also susceptible to a wind. Even the netted fences could be vibrated by a wind, resulting in disturbance on the fiber cable. Under these circumstances, a variation in optical power would be produced for sure.

B. Determination of Thresholds

To simulate an intrusion case and a non intrusion case in this study, we vibrated the netted fences to generate vibration amplitudes of 6 cm and 2 cm, respectively. These two vibration amplitudes corresponded to cases of heavily vibrating the fiber

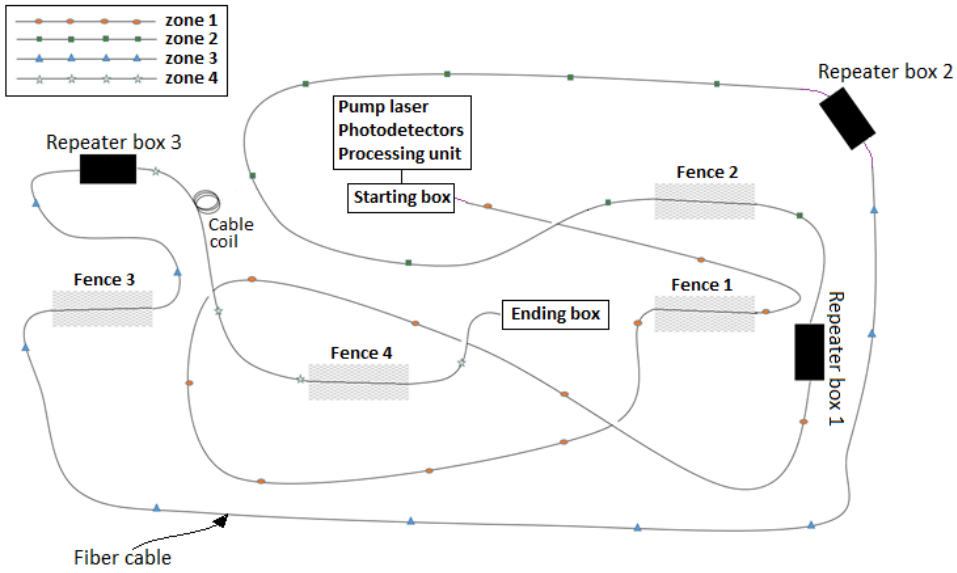

Fig. 5. Fiber cable deployment of a four-perimeter zone intrusion detection system in an outdoor environment. Each zone has a small part of fiber cable attached on a netted fence. Only one single-mode fiber in the fiber cable was used for intrusion detection in each perimeter zone.

(a)

(b)

Fig. 6. Netted fences built outdoors for the experiment. The fences for zones1, 2 and 4 (in (a)) are of 90cm (W) x 50 cm(H); while the fence for zone 3 (in (b)) is of 120 cm (W) x 70 cm(H).

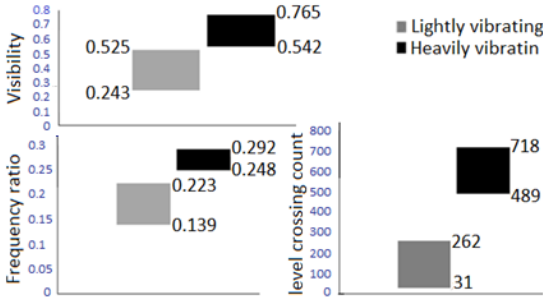

Fig. 7. Ranges of Visibility, FR (frequency ratio) and LCC (level crossing count) for zone 1.

cable and lightly vibrating the fiber cable, respectively. The reason why we chose $v_{\text{low}} = 3000$ Hz, and $v_{\text{high}} = 5000$ Hz for calculation of FR (frequency ratio) was that FR could be quite different as we lightly and heavily vibrated the netted fences, respectively.

We vibrated each netted fence lightly and heavily for a time period of >100 seconds to generate, respectively, 100 time-domain disturbance signals. These signals were recorded and analyzed to give the values of Visibility, FR (frequency ratio) and LCC (level crossing count). These parameter values all fell into different ranges, as shown below.

1) Defended Zone 1: Figure 7 shows the ranges of the three parameters for defended zone 1 when the fiber cable attached on the fence of this zone was lightly vibrated and heavily vibrated separately for >100 seconds. It can be seen that Visibility stayed between 0.542 and 0.765 as the fence was vibrated heavily. When the fiber cable was lightly vibrated, Visibility fell into a range at a lower level. In all figures showing ranges below, the upper and lower bounds of each range are indicated by the numbers shown aside. It can be seen that the two ranges for Visibility in the cases of lightly and heavily vibrating the fence were separable. Therefore, if we set the threshold for Visibility to be 0.535, the upper bound for the case of lightly vibrating would not exceed it, while all Visibilty values were larger than this threshold for the case of heavily vibrating. In this case, as an intruder vibrated the fence, the disturbance signal returning from zone 1 would generate a value of Visibility that exceeded the threshold. On the other hand, when a nonintruding source made a light vibration, the value of Visibility would not exceed the threshold. Figure 8

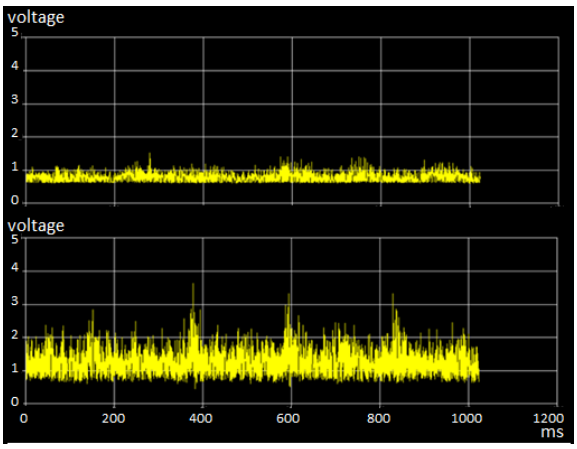

Fig. 8. Detected signal waveforms for the cases of lightly vibrating the fence (upper trace) and heavily vibrating the fence (lower trace) of zone 1.

shows the disturbance signal waveforms for the cases of lightly (upper trace) and heavily (lower trace) vibrating the fence of zone 1. Clearly seen is the larger oscillation amplitude and higher interference visibility for the case of heavily vibrating the fence than for the case of lightly vibrating the fence.

Also we can see that FR and LCC fell into ranges at a higher level when the fence was heavily vibrated than in the case when the fence was lightly vibrated. And notably, lightly vibrating and heavily vibrating the fence led to separate ranges for both FR and LCC, as is illustrated by Fig. 7. Thus, one may set the thresholds for FR and LCC to be 0.235 and 350, respectively. The two waveforms in Fig.8 and their respective Fourier transforms (not shown here) gave Visibility = 0.284, FR = 0.168 and LCC = 175 for the case of light vibration, and Visibility = 0.656, FR = 0.291 and LCC = 716 for the case of heavy vibration. Therefore, such thresholds ensured that heavily vibrating the fence of zone 1 caused Visibility, FR and LCC all to exceed their respective thresholds, and that none of the three parameters would exceed their respective thresholds if the fence was lightly vibrated. An alarm would then go off if the fence was heavily vibrated, while lightly vibrating the fence would not trigger an alarm.

2) Defended Zone 2: The fence of defended zone 2 was also lightly and heavily vibrated for a time period of >100 seconds, respectively, to determine thresholds of the three parameters. Visibility, FR and LCC all fell into their respective ranges as shown in Fig.9. It can be seen that the ranges in the cases of lightly vibrating and heavily vibrating the fence do not overlap for Visibility, FR and LCC. One may choose 0.12, 0.245 and 250 to be the thresholds for Visibility, FR and LCC, respectively.

3) Defended Zone 3: Figure 10 shows the detected signal waveforms for the cases of lightly vibrating (upper trace) and heavily vibrating (lower trace) the fence of zone 3. Lightly vibrating the fence only resulted in a small oscillation amplitude while heavily vibrating the fence could cause a much larger oscillation amplitude. This could be also seen from Fig.11, where Visibility ranged from 0.087 (0.443) to 0.158 (0.819) for the case of lightly vibrating (heavily vibrating) the fence. The signal for the heavy vibration case showed

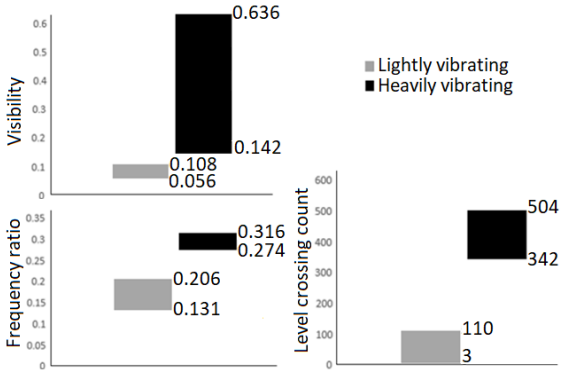

Fig. 9. Ranges of Visibility, FR (frequency ratio) and LCC (level crossing count) for zone 2.

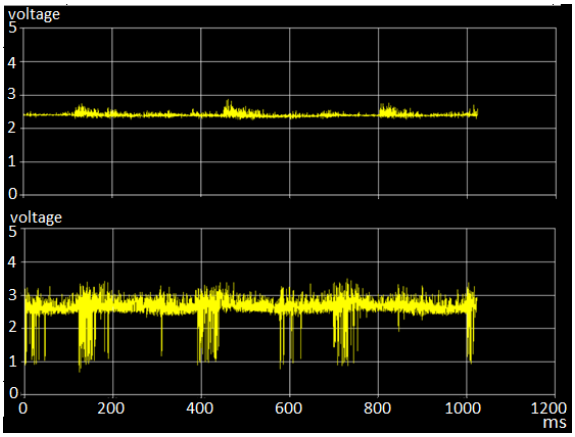

Fig. 10. Detected signal waveforms for the cases of lightly vibrating the fence (upper trace) and heavily vibrating the fence (lower trace) of zone 3.

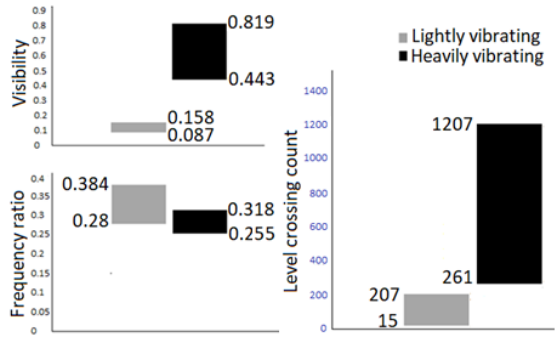

Fig. 11. Ranges of Visibility, FR (frequency ratio) and LCC (level crossing count) for zone 3.

rush-down pulses, resulting in high Visibility. Figure 11 also shows the difference in ranges of LCC for the two vibration cases. With the fence heavily vibrated for >100 seconds, the calculated LCC ranged from 261 to 1207 in contrast to the LCC range of 15 to 207 for a lightly vibrated fence. However, FR shows the opposite result, i.e., the calculated FR stayed in a range at a lower level for the case of heavily vibrating the fence compared with the case of lightly vibrating the fence. To explain this, we calculated the spectra of the signal waveforms shown in Fig.10 by taking a fast Fourier transform operation. The spectra for the upper and lower traces

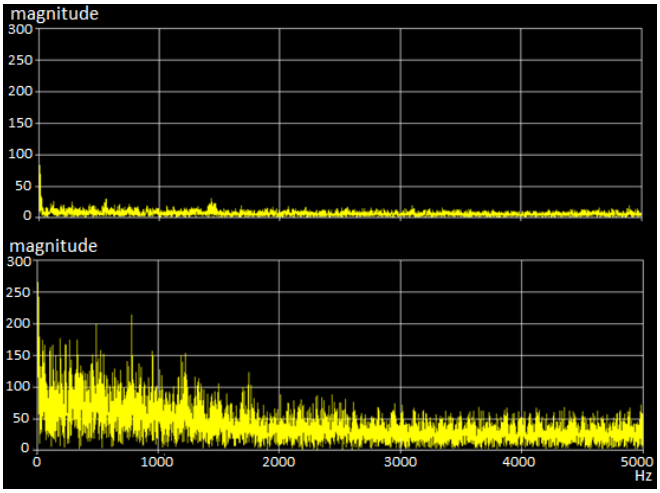

Fig. 12. Fourier spectra of the signal waveforms shown in Fig.10. Upper and lower spectra here correspond to the upper and lower traces of Fig.10, respectively.

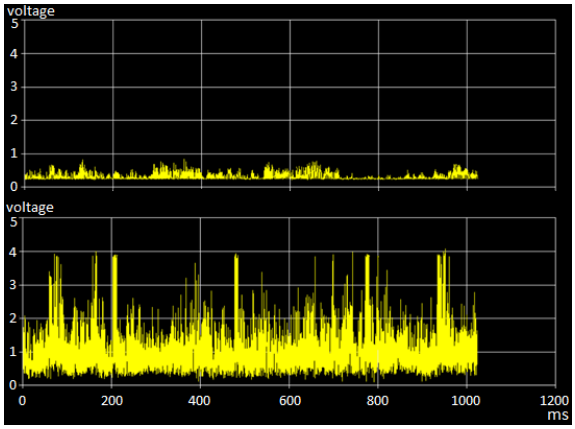

Fig. 13. Detected signal waveforms for the cases of lightly vibrating the fence (upper trace) and heavily vibrating the fence (lower trace) of zone 4.

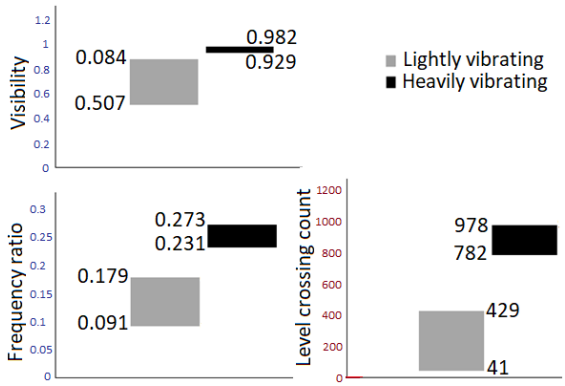

Fig. 14. Ranges of Visibility, FR (frequency ratio) and LCC (level crossing count) for zone 4.

of Fig.10 are shown by the upper and lower spectra in Fig. 12, respectively. From the upper spectrum of Fig.12, we can see that the absolute amplitudes of low-frequency spectral components (except those components near DC) were about identical to those of high-frequency spectral components. However, the low-frequency spectral components had larger absolute amplitudes than the high-frequency components as the fence was heavily vibrated, as shown by the lower spectrum of Fig.12. Thus, as the fence was heavily vibrated, the integrated spectral strength over the band 3000-5000 Hz occupied a smaller share of the whole spectral strength (excluding the DC), compared with the case when the fence was lightly vibrated.

The thresholds for Visibility, FR and LCC could then be set to be 0.28, 0.24 and 230, respectively, in order to detect an intrusion that was equivalent to the case of heavily vibrating the fence. Although the threshold of 0.24 for FR would make the calculated FR exceed the threshold when the fence was lightly vibrated, the other two parameters, i.e., Visibility and LCC, did not exceed the threshold in this case. Therefore, an alarm would not go off when the fence was lightly vibrated. On the other hand, when the fence was heavily vibrated, all of the three parameters exceeded their respective thresholds, and the alarm for intrusion alert would accordingly go off in this case.

4) Defended Zone 4: The two signal waveforms shown in Fig.13 are the detected waveforms when the fence of zone 4 was lightly vibrated (upper trace) and heavily vibrated (lower trace). The unperturbed voltage level for the fiber stayed at ∼0.2 V. It can be seen that the disturbance on the fiber induced a strong oscillation for the detected signal (see the lower trace), as the fence was heavily vibrated, in contrast to the case when the fence was lightly vibrated (see the upper trace). Again the fence was lightly vibrated and heavily vibrated for a time period of >100 seconds, respectively, and the calculated Visibility, FR and LCC were shown in their respective ranges as shown in Fig.14. From this figure, we can see the two ranges for, respectively, light vibration and heavy vibration for each of the three parameters were separable, indicating that a threshold could be determined at some value between the two ranges. One could set the thresholds to be 0.9 (for Visibility), 0.225 (for FR), and 600 (for LCC), and thus vibrating lightly the fence would not be determined as an intrusion while vibrating heavily the fence would.

5) Intrusion Detection Rate and False Alarm Rate: After setting thresholds for the three parameters for each defended zone, we then vibrated the fence of each defended zone consecutively for a time period of 120 seconds. When each of the four fences was lightly vibrated, no intrusion was determined. When a fence was heavily vibrated, however, an intrusion was detected for the corresponding zone only, indicating that there was no cross interference between defended zones and the intrusion detection was quite accurate for each defended zone. Here, we only show the signal waveforms detected for zones 1, 2, and 3 (see Fig.15) when the fence of zone 4 was heavily vibrated. It can be seen from Fig.15 that the signal waveforms for all the three zones appeared to be almost a constant line. Note that these results were obtained just when there was no wind at the moment of test. The average wind speed on the day of test was 2 m/sec, while a moderate breeze at a speed of ∼5 m/sec came occasionally. A signal waveform detected for zone 1 when such a breeze came is shown in Fig. 16, where an oscillation in waveform is apparent. The calculated

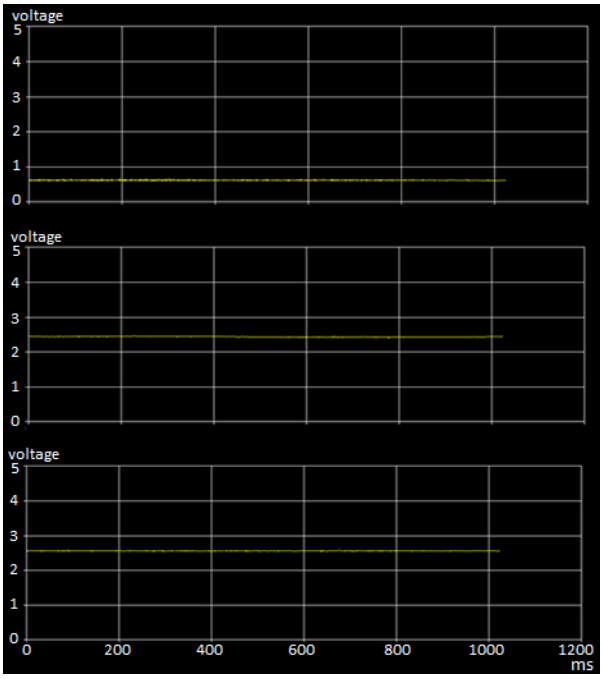

Fig. 15. Detected signal waveforms for zones 1 (top), 2 (middle) and 3 (bottom) when the fence of zone 4 was heavily vibrated.

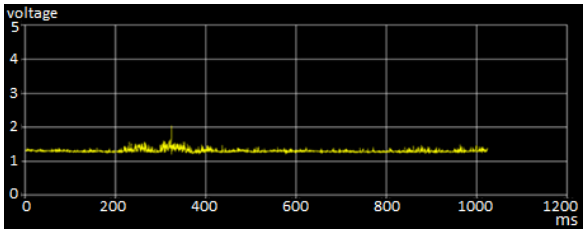

Fig. 16. Detected signal waveform for zone 1 when a breeze at the speed of ~ 5 m/sec came to the test field.

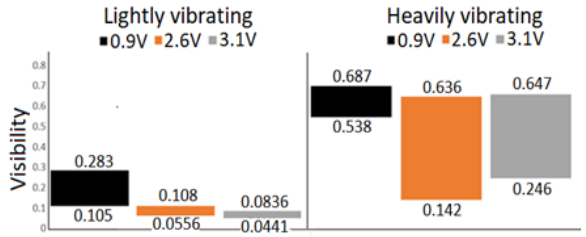

Fig. 17. Ranges over which Visibility was distributed with the fence of zone 2 lightly vibrated and heavily vibrated separately for a time period of >100 seconds.

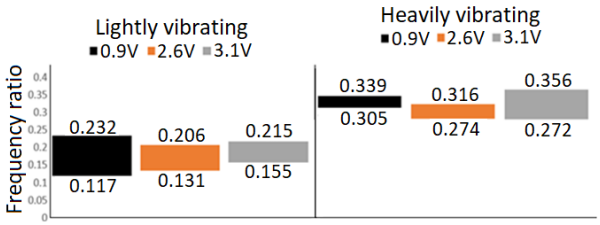

Fig. 18. Ranges over which FR (frequency ratio) was distributed with the fence of zone 2 lightly vibrated and heavily vibrated separately for a time period of >100 seconds.

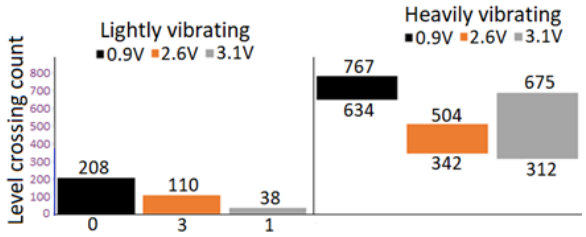

Fig. 19. Ranges over which LCC (level crossing count) was distributed with the fence of zone 2 lightly vibrated and heavily vibrated separately for a time period of >100 seconds.

Visibility, FR and LCC were 0.26, 0.265 and 31, respectively, for this case. Such a wind gave rise to a Visibility and an LCC that were both lower than their respective thresholds. Nevertheless, the FR value was higher than the threshold 0.235. However, the calculated Visibility, FR and LCC did not exceed the thresholds simultaneously, and thus no intrusion was determined in this case.

Since disturbance signals were analyzed every 1.024 second in our study, the response time for determining an intrusion would be 1.024 second plus the time period required for computing. However, the computing for determining an intrusion would only take a small fraction of a second, as we observed that an alarm alert appeared promptly on the computer screen once any fence was heavily vibrated.

6) Effect of Temperature: Even when the fiber was not vibrated, the output signal level (denoted as reference voltage level RVL here) for the unperturbed laser cavity and extended resonator could change with the environmental temperature because of the temperature-induced phase variation on the light propagating through the fiber. The effect of RVL was studied previously in [28] for the structure of Michelson interferometer. Here we took defended zone 2 for example to see the effect of RVL on the intrusion detection. Note that when the environmental temperature varies, a change in the offset phase between the lights from the laser cavity and the extended resonator would arise, thus leading to an output signal level (i.e., RVL) staying at a voltage level that varies with temperature. On the day of test, the temperature dropped from 35 °C at noon to 30 °C at 6 PM, causing the RVL to move from 2.5 V to 1.75 V.

Here for defended zone 2, we measured Visibility, FR and LCC for RVL levels of 0.9 V, 2.6 V and 3.1 V, respectively. To make a particular RVL, we intentionally strained the fiber by slightly bending the fiber cable lying on the grass, and then calculated Visibility, FR and LCC. Figures 17, 18 and 19 show the ranges for Visibility, FR and LCC, respectively, as the fence was lightly vibrated and heavily vibrated separately for a time period of >100 seconds. One can see from Fig.17 that Visibility ranged from 0.105 to 0.283 for RVL = 0.9 V in the case of lightly vibrating the fence, which means Visibility could exceed the threshold 0.12 sometimes for this RVL. Figure 17 also indicates that Visibility always exceeded the threshold 0.12 for any RVL as the fence was heavily vibrated. The threshold of 0.245 for FR was always higher than the calculated FR values for any RVL in the case of lightly vibrating the fence, while the calculated FR values always exceeded

TABLE I
COMPARISON OF VARIOUS TECHNOLOGIES FOR INTRUSION DETECTION

Technology	Number of fibers used in fiber cable	Length of total protected area	Spatial resolution	Type of light source used
FBG	1	100 m [1]	3~5 m [1]	broadband swept laser
Φ-OTDR	1	could be >100 km (e.g.,131.5 km [19])	pulsewidth dependent (e.g., 8 m [19])	highly coherent laser
Michelson interferometer	2	4.012 km [4]	±45 m[4]	two DFB lasers at different wavelengths
Sagnac interferometer	2*	180 m[9]; 10 km[10]	1 m [9]; 400 m [10]	broadband [9,10]
Dual Mach-Zehnder interferometer	3	61 km [8]	52.5 m [8]	DFB laser
Merged interferometers	2	180 m [11]; 100m [12]; 200m [13]	2.7 m [11]; 0.6 m [12]; 5 m [13]	laser[11~13]
Multi-zone[21]	4	source power dependent	zone length	intensity modulated, broadband
Multi-zone[22]	3	source power dependent	zone length	multi-wavelength laser
Multi-zone[23]	N**	N x 500 m	up to 500 m	broadband
Multi-zone[24]	2***	4 times zone length	zone length	980 nm pump laser
Multi-zone[25]	3	source power dependent	zone length	broadband
Multi-zone [28,29]	3 [28], 2 [29]	pump power dependent	zone length	1480 nm pump laser
The proposed	1	pump power dependent	zone length	1480 nm pump laser

* This is the case when the protected zone is arranged in a line.
** N is equal to the number of protected zones if these zones are cascaded in a line pattern. Different wavelengths are allocated for the protected zones.
*** Only 4 zones can be protected. The fibers used are not single-mode fibers, but erbium-doped fibers.

this threshold for any RVL in the case of heavily vibrating the fence, as shown in Fig.18. Figure 19 demonstrates a similar story for LCC. In short summary, lightly vibrating the fence for any RVL would not cause an alarm for intrusion alert, while heavily vibrating the fence would.

IV. CONCLUSION

We have presented for the first time a new fiber-optic system for multiple-perimeter-zone intrusion detection employing only one single-mode fiber simultaneously as a disturbance sensor and a light transmission medium for each defended zone. A pump laser delivered its power to pump a section of erbium-doped fiber in a laser cavity for each defended zone, with the gain medium also supporting an extended resonator. An interference signal aroused by the beat between the lights from the laser cavity and the extended resonator was then produced. Oscillation of the interference signal was then detected and three parameters corresponding to the signal waveform recorded in every 1.024-second time period were calculated. Visibility, frequency ratio (FR) and level crossing count (LCC) were accordingly obtained. In an outdoor test, we simulated the cases of a nonintrusion and an intrusion for each defended zone by lightly vibrating and heavily vibrating the fence, respectively, and determined the thresholds for the three parameters. The three thresholds were preset for each defended zone, and the three calculated parameters for a defended zone must all exceed their respective thresholds to declare an intrusion for that defended zone. Experiments have demonstrated that there were no cross interference between any two defended zones, and that a zero false alarm rate as well as a 100 % alarm-upon-intrusion rate could be reached for any defended zone based on the way these fences were vibrated.

Although only four defended zones were set for study, the number of zones can be extended to such an extent that the erbium-doped fiber in the last defended zone acquires sufficient pump power to generate sufficient signal laser power. For example, if each defended zone needs a pump power of 10 mW (considering losses resulting from optical components, especially the DWDM filter), then a 160 mW/320 mW pump laser would be able to supply power to 16/32 defended zones. When more losses have to be taken into account, e.g., a loss resulting from splicing, more pump power is then required.

Use of only one single-mode fiber for disturbance sensing could give some advantages. First, a fiber cable with only one single-mode fiber is cost-effective than multi-core cables. Most importantly, as a great number of defended zones are to be constructed for a long range of perimeter, we can use each fiber in an M-core cable for an N-perimeter-zone detection system, with a pump laser used for such N-perimeter-zone detection. In this case, a total number of MxN defended zones can be implemented with M pump lasers used. Taking an example of $M = 12$ and $N = 32$, we can have 384 defended zones constructed in a line pattern with a cable of twelve single mode fibers (i.e., 12-core fiber cable) used.

Finally, we compare various intrusion detection techniques including those mentioned in this paper and the proposed in terms of the number of fibers used, length of the total protected area, spatial resolution, and the type of light source used. The comparison is given in Table I. We can see from the table that the proposed work presents a unique technique in which only one single-mode fiber is used for multi-zone intrusion detection. Also, it can be noted that the length of the protected area is optical power dependent for multi-zone detection systems. However, many multi-zone systems can support perimeter detection over a long-length perimeter zone as long as their power sources deliver enough optical power.

REFERENCES

[1] H. Wu, Y. Rao, C. Tang, Y. Wu, and Y. Gong, "A novel FBG-based security fence enabling to detect extremely weak intrusion signals from nonequivalent sensor nodes," *Sens. Actuators A, Phys.*, vol. 167, no. 2, pp. 548–555, Jun. 2011.

[2] Y. Chen, L.-X. Zhou, and H.-L. Liu, "A fiber Bragg grating sensor perimeter intrusion localization method optimized by improved particle swarm optimization algorithm," *IEEE Sensors J.*, vol. 18, no. 3, pp. 1243–1249, Feb. 2018.

[3] M. Kezmah, D. Donlagic, and B. Lenardic, "Low cost security perimeter based on a Michelson interferometer," in *Proc. IEEE Sensors Conf.*, Oct. 2008, pp. 1139–1142.
[4] X. Hong, J. Wu, C. Zuo, F. Liu, H. Guo, and K. Xu, "Dual Michelson interferometers for distributed vibration detection," *Appl. Opt.*, vol. 50, no. 22, pp. 4333–4338, Aug. 2011.
[5] Q. Li, H. Wang, L. Li, S. Liang, and X. Zhong, "Fiber-optic sensor based on Michelson interferometers for distributed disturbance detection," *Infr. Laser Eng.*, vol. 44, no. 1, pp. 205–209, Jan. 2015.
[6] G. Luo *et al.*, "Distributed fiber optic perturbation locating sensor based on dual Mach–Zehnder interferometer," *Proc. SPIE*, vol. 6622, Feb. 2008, Art. no. 66220Z.
[7] Q. Chen *et al.*, "An elimination method of polarization-induced phase shift and fading in dual Mach–Zehnder interferometry disturbance sensing system," *J. Lightw. Technol.*, vol. 31, no. 19, pp. 3135–3141, Oct. 1, 2013.
[8] C. Ma *et al.*, "Long-range distributed fiber vibration sensor using an asymmetric dual Mach–Zehnder interferometers," *J. Lightw. Technol.*, vol. 34, no. 9, pp. 2235–2239, May 1, 2016.
[9] X. Fang, "A variable-loop Sagnac interferometer for distributed impact sensing," *J. Lightw. Technol.*, vol. 14, no. 10, pp. 2250–2254, Oct. 1, 1996.
[10] W. Xu, C. Zhang, S. Liang, L. Li, W. Lin, and Y. Yang, "Fiber-optic distributed sensor based on a Sagnac interferometer with a time delay loop for detecting time-varying disturbance," *Microw. Opt. Technol. Lett.*, vol. 51, no. 11, pp. 2564–2567, Nov. 2009.
[11] S. J. Spammer, P. L. Swart, and A. A. Chtcherbakov, "Merged Sagnac–Michelson interferometer for distributed disturbance detection," *J. Lightw. Technol.*, vol. 15, no. 6, pp. 972–976, Jun. 1997.
[12] A. A. Chtcherbakov, P. L. Swart, and S. J. Spammer, "Mach–Zehnder and modified Sagnac-distributed fiber-optic impact sensor," *Appl. Opt.*, vol. 37, no. 16, pp. 3432–3437, Jul. 1998.
[13] A. A. Chtcherbakov, P. L. Swart, S. J. Spammer, and B. M. Lacquet, "Modified Sagnac/Mach–zehnder interferometer for distributed disturbance sensing," *Microw. Opt. Technol. Lett.*, vol. 20, no. 1, pp. 34–36, Jan. 1999.
[14] Y. C. Hsu, "Study of intrusion detection and location using dual Mach–Zehnder interferometers with fiber laser as light source: Locating two different places of intrusion at the same time," M.S. thesis, Inst. Photon. Tech., Nat. Tsing Hua Univ., Hsinchu, Taiwan, 2019.
[15] [Online]. Available: http://www.fftsecurity.com/wp-content/uploads/FFT-Secure-Fence-Product_Secification.pdf
[16] J. C. Juarez, E. W. Maier, K. N. Choi, and H. F. Taylor, "Distributed fiber-optic intrusion sensor system," *J. Lightw. Technol.*, vol. 23, no. 6, pp. 2081–2087, Jun. 2005.
[17] Y. Lu, T. Zhu, L. Chen, and X. Bao, "Distributed vibration sensor based on coherent detection of phase-OTDR," *J. Lightw. Technol.*, vol. 28, no. 22, pp. 3243–3249, Nov. 2010.
[18] A. Masoudi, M. Belal, and T. P. Newson, "A distributed optical fibre dynamic strain sensor based on phase-OTDR," *Meas. Sci. Technol.*, vol. 24, no. 8, Jul. 2013, Art. no. 085204.
[19] F. Peng, H. Wu, X.-H. Jia, Y.-J. Rao, Z.-N. Wang, and Z.-P. Peng, "Ultra-long high-sensitivity Φ-OTDR for high spatial resolution intrusion detection of pipelines," *Opt. Exp.*, vol. 22, no. 11, pp. 13804–13810, Jun. 2014.
[20] M. Aktas, T. Akgun, M. U. Demircin, and D. Buyukaydin, "Deep learning based multi-threat classification for phase-OTDR fiber optic distributed acoustic sensing applications," *Proc. SPIE*, vol. 10208, Apr. 2017, Art. no. 102080G.
[21] A. D. Meyer, "Sensor array for perimeter defense," U.S. Patent 7 526 147 B2, Apr. 28, 2009.
[22] P. A. Townley-Smith, S. Hellman, J. Kondis, and E. R. Ranalli, "Perimeter detection using fiber optic sensors," U.S. Patent 7 488 929 B2, Feb. 10, 2009.
[23] X. Li, Q. Sun, J. Wo, M. Zhang, and D. Liu, "Hybrid TDM/WDM-based fiber-optic sensor network for perimeter intrusion detection," *J. Lightw. Technol.*, vol. 30, no. 8, pp. 1113–1120, Apr. 15, 2012.
[24] S.-L. Woon, K.-M. Kwan, W.-Y. Chong, H.-S. Lin, and C.-H. Pua, "Cascaded acoustic wave sensors based on erbium-doped fiber laser dynamics for intrusion zone identification," *IEEE Sensors J.*, vol. 17, no. 6, pp. 1893–1897, Mar. 2017.
[25] J. Tian, Y. Zhou, and H. Zhao, "One-cable optical fiber vibration alarm system," China Patent 104 913 840 B, Nov. 10, 2017. [Online]. Available: https://worldwide.espacenet.com/patent/search/family/054083101/publication/CN104913840B?called_by=epo.org&q=CN%2010491 3840%20B
[26] S. S. Mahmoud and J. Katsifolis, "Robust event classification for a fiber optic perimeter intrusion detection system using level crossing features and artificial neural networks," *Proc. SPIE*, vol. 7677, Apr. 2010, Art. no. 767708.
[27] S. S. Mahmoud, Y. Visagathilagar, and J. Katsifolis, "Real-time distributed fiber optic sensor for security systems: Performance, event classification and nuisance mitigation," *Photonic Sensors*, vol. 2, no. 3, pp. 225–236, Sep. 2012.
[28] K.-S. Lin, K.-H. Yeh, Y.-J. Chiang, and L. Wang, "Fiber-optic perimeter intrusion detection by employing a fiber laser cavity in each defensed zone," *IEEE Sensors J.*, vol. 18, no. 20, pp. 8352–8360, Oct. 2018.
[29] H. Hsieh, K.-S. Hsu, T.-L. Jong, and L. Wang, "Multi-zone fiber-optic intrusion detection system with active unbalanced Michelson interferometer used for security of each defended zone," *IEEE Sensors J.*, vol. 20, no. 3, pp. 1607–1618, Feb. 2020.

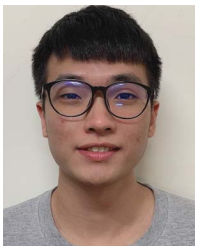

Yuan-Hung Lin was born in Taiwan, in 1996. He received the B.S. degree in electronic engineering from Chang Gung University, Taiwan, in 2018, and the M.S. degree in photonics technology from National Tsing Hua University, Hsinchu, Taiwan, in 2020. He is currently providing his four-month military service for the government. His research interests include optical fiber sensors and numerical computation with computer.

Bo-Hong Zheng was born in Taiwan, in 1997. He received the B.S. degree in electrical engineering from I-Shou University, Taiwan, in 2019. He is currently pursuing the M.S. degree with the Institute of Photonics Technologies, National Tsing Hua University, Hsinchu, Taiwan. His research interests include optical fiber sensors and programming with computer language such as C++ and python.

Likarn Wang was born in Taiwan, in 1959. He received the B.S. and M.S. degrees in electrical engineering from National Tsing Hua University, Hsinchu, Taiwan, in 1981 and 1983, respectively, and the Ph.D. degree in electrical engineering from Pennsylvania State University, University Park, PA, USA, in 1989. In 1990, he started working with the Department of Electrical Engineering, National Tsing Hua University, as an Associate Professor, where he became a Full Professor in 1998. Then, he joined the Institute of Photonics Technologies, National Tsing Hua University, in 2003. He was named the Director of the Institute of Photonics Technologies in 2012 and took a three-year term position. His research interests include optical fiber sensors, waveguide optics, and solar cells.